Ecotoxicology and Environmental Safety 276 (2024) 116284

Contents lists available at ScienceDirect

Ecotoxicology and Environmental Safety

journal homepage: www.elsevier.com/locate/ecoenv

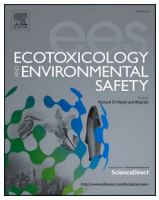

Protective effects of sodium butyrate on fluorosis in rats by regulating bone homeostasis and serum metabolism

Ying Li [a,1], Fengmei Yang [a,b,1], Jie Liu [a,1], Mengqi Jiang [a], Ye Yu [a], Qingyi Zhou [a], Lu Sun [c,*], Zhuo Zhang [a,*], Lin Zhou [a,*]

[a] School of Public Health, Shenyang Medical College, Shenyang 110034, China
[b] Yulin Center for Disease Control and Prevention, Yulin Municipal Health Committee, Yulin 719100, China
[c] Radiation Health Center, Liaoning Provincial Center for Disease Control and Prevention, Shenyang 110015, China

ARTICLE INFO

Edited by: Yong Liang

Keywords:
Sodium butyrate
Fluorosis
Bone homeostasis
Serum metabolism

ABSTRACT

Fluorosis due to high fluoride levels in drinking water profoundly affects the development of human skeletal and dental structures. Sodium butyrate (NaB) has been found to regulate overall bone mass and prevent pathological bone loss. However, the mechanism of NaB action on fluorosis remains unclear. In this study, a rat model of fluorosis induced by 100 mg/L sodium fluoride was used to investigate the impact of NaB on bone homeostasis and serum metabolomics. It was found that NaB significantly reduced the levels of bone resorption markers CTX-I and TRACP-5B in fluorosis rats. Moreover, NaB increased calcium and magnesium levels in bone, while decreasing phosphorus levels. In addition, NaB improved various bone microstructure parameters, including bone mineral density (BMD), trabecular thickness (Tb. Th), trabecular bone separation (Tb. SP), and structural model index (SMI) in the femur. Notably, NaB intervention also enhanced the antioxidant capacity of plasma in fluorosis rats. Furthermore, a comprehensive analysis of serum metabolomics by LC-MS revealed a significant reversal trend of seven biomarkers after the intervention of NaB. Finally, pathway enrichment analysis based on differential metabolites indicated that NaB exerted protective effects on fluorosis by modulating arginine and proline metabolic pathways. These findings suggest that NaB has a beneficial effect on fluorosis and can regulate bone homeostasis by ameliorating metabolic disorders.

1. Introduction

Fluoride is an essential trace element that plays a vital role in human metabolic processes. Ingestion of fluoride through drinking water is often the primary source of fluoride intake for individuals (Podgorski and Berg, 2022). According to the World Health Organization. (2017), low concentrations of fluoride (0.5–1.0 ppmv) in drinking water can help prevent dental caries, while high concentrations (>1.5 ppmv) can lead to fluorosis.

Fluorosis can cause different degrees of lesions in various tissues and organs of the whole body, mainly including bone-phase and non-bone-phase damage. Among them, bone phase damage is primarily skeletal fluorosis involving joints such as the neck, shoulders, knees, and hips, resulting in significant stiffness and pain that can affect individuals of all ages (Yadav et al., 2023). Unfortunately, there has been a lack of effective prevention and treatment for skeletal fluorosis, despite the fact that the symptoms can make the patient's health condition progressively worse and irreversible (Srivastava and Flora, 2020a).

Recent studies have indicated that skeletal fluorosis development is associated with oxidative stress and endoplasmic reticulum stress (Garcia et al., 2021; Shashi and Thakur, 2022), overexpression or imbalance of local regulatory networks of bone metabolism and related factors (Collins et al., 2022). As with many chronic degenerative diseases, fluoride-induced oxidative stress is considered a key mechanism by which fluoride exposure produces various toxic effects (Babu et al., 2022). Fluorosis leads to excessive production of reactive oxygen species, which can interfere with bone cell metabolism and inhibit normal bone cell functions, further promoting the development of skeletal fluorosis (Jin et al., 2023).

Short-chain fatty acids (SCFA) are highly regarded metabolites produced by gut microorganisms and play an important role in the regulation of body metabolism. Recent studies have shown that SCFA exerted

* Corresponding authors.
E-mail addresses: sunlu0222@aliyun.com (L. Sun), zhangzhuo@symc.edu.cn (Z. Zhang), zhoulin@symc.edu.cn (L. Zhou).
[1] Ying Li, Fengmei Yang and Jie Liu are co-first authors of the article.

https://doi.org/10.1016/j.ecoenv.2024.116284
Received 4 January 2024; Received in revised form 16 March 2024; Accepted 30 March 2024
Available online 5 April 2024

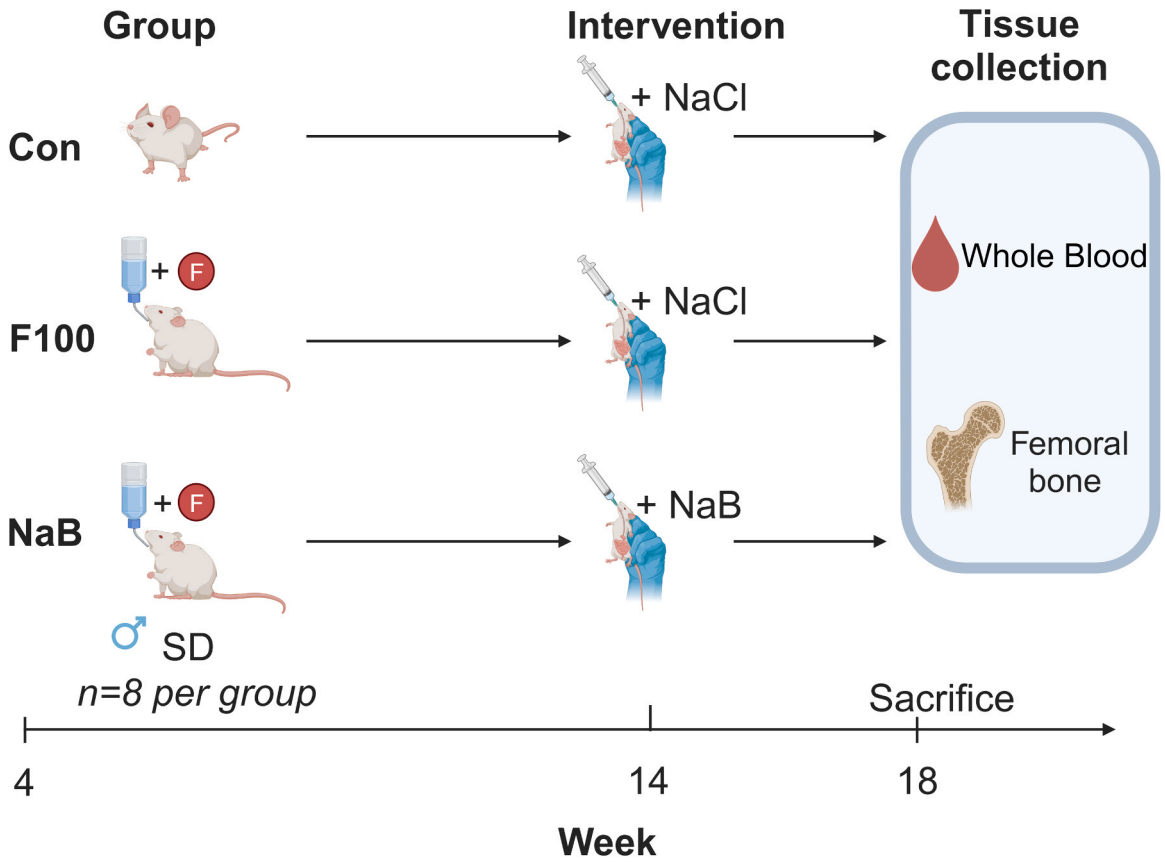

Fig. 1. Experimental schedule. 24 SD male rats were divided into three groups of 8 rats each: Con group (distilled water), F100 group (Fluorosis group at 100 mg/L NaF), and NaB group (1000 mg/kg/d NaB+100 mg/L NaF).

important regulatory effects on bone development and bone metabolism-related disease (Lucas et al., 2018a; Montalvany-Antonucci et al., 2019). As an important member of the SCFA family, butyrate and its salts can improve bone mass and enhance bone microstructures *in vivo* and *in vitro* (Tang et al., 2020a; Liu et al., 2023c). As early as 1993, Iwami and Moriyama demonstrated that sodium butyrate (NaB) could promote the proliferation and metabolic function of osteoblasts and enhance alkaline phosphatase (ALP) activity (Iwami and Moriyama, 1993). Subsequently, it was found that NaB stimulated bone formation by increasing the production of bone sialoprotein and osteopontin while inhibiting osteoclast differentiation by increasing the production of osteoprotegerin by human osteoblasts. (Katono et al., 2008). Moreover, Tang *et al.* (Tang et al., 2020b) revealed that NaB prevented osteoporosis in rats by promoting periosteal GSK-3β/Nrf2 signaling and mitochondrial function. Additionally, NaB treatment could enhance ALP activity, mineralization capacity, and Coll-I, BMP2, and OCN expression levels in MC3T3-E1 cells, whereas also suppressing PKC and NF-κB expressions, intracellular ROS production and malondialdehyde levels within the cytosol (Liu et al., 2023d). Meanwhile, an increase in bone mineral density was found in NaB-treated rats (Liu et al., 2023d). Therefore, NaB is hypothesized to play an important role in the prevention and treatment of bone homeostasis imbalance and bone metabolism disorders caused by fluorosis. However, its exact mechanism for the treatment of fluorosis remains unclear.

Fluorosis-induced bone damage is a disorder of bone tissue metabolism that is closely related to changes in metabolites. Serum, as a readily available biofluid containing a variety of endogenous small molecule metabolites, has become an important indicator of physiological and pathological status (Zhang et al., 2012). Wang et al. (2019a) identified that several metabolites in serum were associated with bone mineral density. Moreover, a recent study based on serum metabolomics found that puerarin improved OVX-induced osteoporosis by regulating phospholipid metabolism and unsaturated fatty acid biosynthesis (Li et al., 2022). Therefore, it can be concluded that research based on serum metabolomics contributes to a comprehensive understanding of the effects of NaB on bone metabolism in rats with fluorosis.

This study aims to comprehensively investigate how NaB affects bone homeostasis and serum metabolism to alleviate fluoride poisoning. First, the levels of bone resorption markers, bone mineral content, bone microstructure parameters, and plasma biochemical indicators were determined to assess the impact of NaB on bone health indicators and structure. Furthermore, serum metabolites were systematically analyzed by LC-MS and pathway enrichment based on differential metabolites was performed to reveal the metabolic pathways of NaB for alleviating fluorosis. This will provide a theoretical basis for NaB to prevent the occurrence of fluorosis and lay the foundation for the use of NaB as a new therapeutic approach for fluorosis in the clinic.

2. Materials and methods

2.1. Chemicals and reagents

NaB (purity ≥ 98.5%) was acquired from Sigma (MO, USA) and NaF (purity 98%) was purchased from Shanghai McLean Biochemical Technology Co (Shanghai, China). Rat osteocalcin (OCN) ELISA kit, rat collagen type I C-terminal peptide (CTX-I) ELISA kit, and rat anti-tartrate acid phosphatase 5B (TRACP-5B) ELISA kit were obtained from Nanjing Jiancheng Bioengineering Institute (Nanjing, China).

2.2. Animals and treatment

All animal experiments were approved by the Laboratory Animal

Ethics Committee of Shenyang Medical College (No. SYYXY2019040602). A total of twenty-four male Sprague-Dawley (SD) rats, aged three weeks, with an average weight of 60±5 g, were purchased from Liaoning Changsheng Biological Company (Liaoning, China). The rats were housed in a standard laboratory environment with a temperature of 23±2℃, relative humidity of 50–70%, and a light/dark cycle of 12 h each.

After one week of acclimatization feeding, the rats were randomly divided into three groups of 8 rats each based on body weight. During the experiment, rats in the control group (Con) were given distilled water for the entire duration of the experiment, while the rats in the fluorosis group (F100) and the NaB group were provided with a 100 mg/L solution of sodium fluoride (NaF). The dosage of sodium fluoride was selected based on previous studies (Wang et al., 2020; Zhong et al., 2021) and preliminary experiments. After ten weeks of fluoride exposure, rats in the Con and F100 groups were administered a 0.9% NaCl solution by gavage, while rats in the NaB group received NaB at a concentration of 1000 mg/kg/d by gavage once a day for four weeks (Fig. 1). The final dose and cycle of NaB administration were according to previous studies (Egorin et al., 1999; Yang et al., 2014; Liu et al., 2015; Khan and Jena, 2016) and pre-experiments.

The body weight, mental status, food consumption, and metabolite status of the rats were monitored daily throughout the experiment. At the end of the experiment, the rats were anesthetized and executed by intraperitoneal injection of 2% sodium pentobarbital, followed by the collection of whole blood from the abdominal aorta and the isolation and preservation of serum and plasma. In addition, the hind limb bones of the rats were removed and preserved at −80°C under freezing conditions.

2.3. Determination of femoral bone mineral content

The calcium, magnesium, and zinc levels in bone minerals were determined by atomic absorption spectrophotometry (AA-7000, Shimadzu, Japan) (Ščančar et al., 2000). The femur was first carbonized to separate its mineral content by removing organic substances. The carbonized bone was heated in a muffle furnace at 550°C for 6 hours and subsequently dissolved in a 65% nitric acid solution. The elemental contents were determined under air-acetylene flame conditions at a wavelength of 213.9 nm for zinc, 285.2 nm for magnesium, and 422.7 nm for calcium. The actual levels of calcium, magnesium, and zinc in the bone mineral were calculated from the calibration curve.

The phosphorus content in the samples was determined using the molybdenum blue colorimetric method (Chen et al., 1956). The determination of phosphorus in the samples was carried out according to the instructions of the phosphate assay kit (Nanjing Jiancheng Bioengineering Institute, Nanjing, China). First, 0.1 mL of the sample was mixed with 0.4 mL of precipitant, followed by centrifugation at 3500 rpm for 10 minutes, and the supernatant was taken for measurement. The sample supernatant or phosphorus standard solution was mixed with the working solution respectively. The mixture was cooled to room temperature after 30 minutes in a water bath at 37℃, and the absorbance was measured at 660 nm.

The fluoride content in the sample solutions was determined by the fluoride ion-selective electrode method (Lei Magnetic, Shanghai, China) (Martínez-Mier et al., 2011). The method is based on the potentiometric response of a fluoride ion-selective electrode to free fluoride ions in solution. First, a series of fluoride standard solutions were prepared, and the fluoride ion-selective electrode and reference electrode were immersed in the standard solution and the sample solution. The stabilized potential values for each solution were accurately measured and recorded using an ion meter. The logarithm of the fluoride ion concentration was used as the x-axis and the potential values as the y-axis to obtain the standard working curve. The fluoride ion concentration of the corresponding sample solution was calculated from the standard curve.

2.4. Micro-computed tomography (micro-CT) analysis

The femoral microstructures were analyzed by micro-CT scanning (SkyScan1276, Bruker, GER). Following 24 h of fixation of the left femur with 40 g/L paraformaldehyde solution, the processed femur was placed vertically into a micro-CT, specimen tube and fixed to prevent dehydration or displacement of the specimen during the scanning process. The scanning parameters were 55 kV voltage, 72 μA current, and a rotation step of 0.4 degrees. The region of interest (ROI) for three-dimensional reconstruction was selected in the area of bone marrow cavity 0.215 mm from the growth plate. The chosen ROI had a thickness of 1.72 mm and the necessary image data was retrieved for the reconstruction process. The acquired images were subjected to quantitative analysis using the system's software. The analysis primarily encompassed the assessment of trabecular bone density (Tb. BMD), bone volume fraction (BV/TV), trabecular bone thickness (Tb. Th), trabecular bone number (Tb. N), trabecular bone separation (Tb. SP), structural model index (SMI), and trabecular bone connectivity density (Conn.Dn).

2.5. Determination of plasma biochemical indicators

The determination of malondialdehyde (MDA) level, catalase (CAT) activity, glutathione peroxidase (GSH-Px) activity, total superoxide dismutase (T-SOD) activity, reduced glutathione (GSH) level, and total antioxidant capacity (T-AOC) level was conducted following the instructions provided by the respective kits (Elabscience Biotech Co, Wuhan, China). For MDA assay, 50 μL of standard solution or sample solution was added to a 96-well plate, followed by 50 μL of biotinylated detection antibody and incubation at 37°C for 45 minutes. After washing, 100 μL of HRP conjugate was added to each well and the mixed system was incubated at 37°C for 30 minutes. Following another wash, the wells were then treated with 90 μL of substrate reagent and incubated at 37°C for 15 min. Finally, 50 μL of termination solution was added to the wells and the absorbance was measured at 450 nm. CAT activity was determined at a wavelength of 405 nm by measuring the residual reaction between H_2O_2 and ammonium molybdate, which forms a yellow complex, indicating the efficacy of CAT in decomposing hydrogen peroxide. Regarding GSH-Px activity, the sample was mixed with the extraction reagent, followed by centrifugation at 500 g for 5 min at room temperature. Then the obtained supernatant was mixed with the corresponding detection reagent, and the absorbance was measured at 412 nm after standing at room temperature for 15 min. T-SOD activity was gauged at 550 nm based on its ability to inhibit the reaction between WST-8 salt and superoxide anions. GSH levels were assessed colorimetrically at a wavelength of 405 nm based on the production of yellow TNB ions by the DTNB reaction. T-AOC levels were measured at 520 nm using spectrophotometry.

2.6. Metabolomics of biological samples by LC/MS

After thawing at room temperature, 400 μL of acetonitrile was added to each 100 μL serum sample to precipitate proteins, followed by an overnight incubation at −20 °C. The precipitated proteins were separated from the supernatant by centrifuging at 20,000 g for 10 minutes. Subsequently, the supernatant was subjected to freeze-drying in preparation for further metabolomics analysis. QCs for the LC/MS analysis were prepared by taking 5 μL aliquots of each treated sample to ensure the reproducibility and validity of the experiments. The separation was performed on an X Bridge BEH C18 column (3.5 μm, 2.1 mm × 100 mm) with gradient elution using a dual-solvent system, which was solvent A (water plus 0.1% formic acid) and solvent B (acetonitrile plus 0.1% formic acid). Gradient elution conditions were as follows: 0–0.5 min, 5% B; 0.5–5 min, 5%-80% B; 5–7 min, 80%-100% B; 7–8 min, 100% B; 8–8.1 min, 100%-5% B; and 8.1–10 min, 5% B.

The temperature of the column was maintained at 50 ℃, the flow

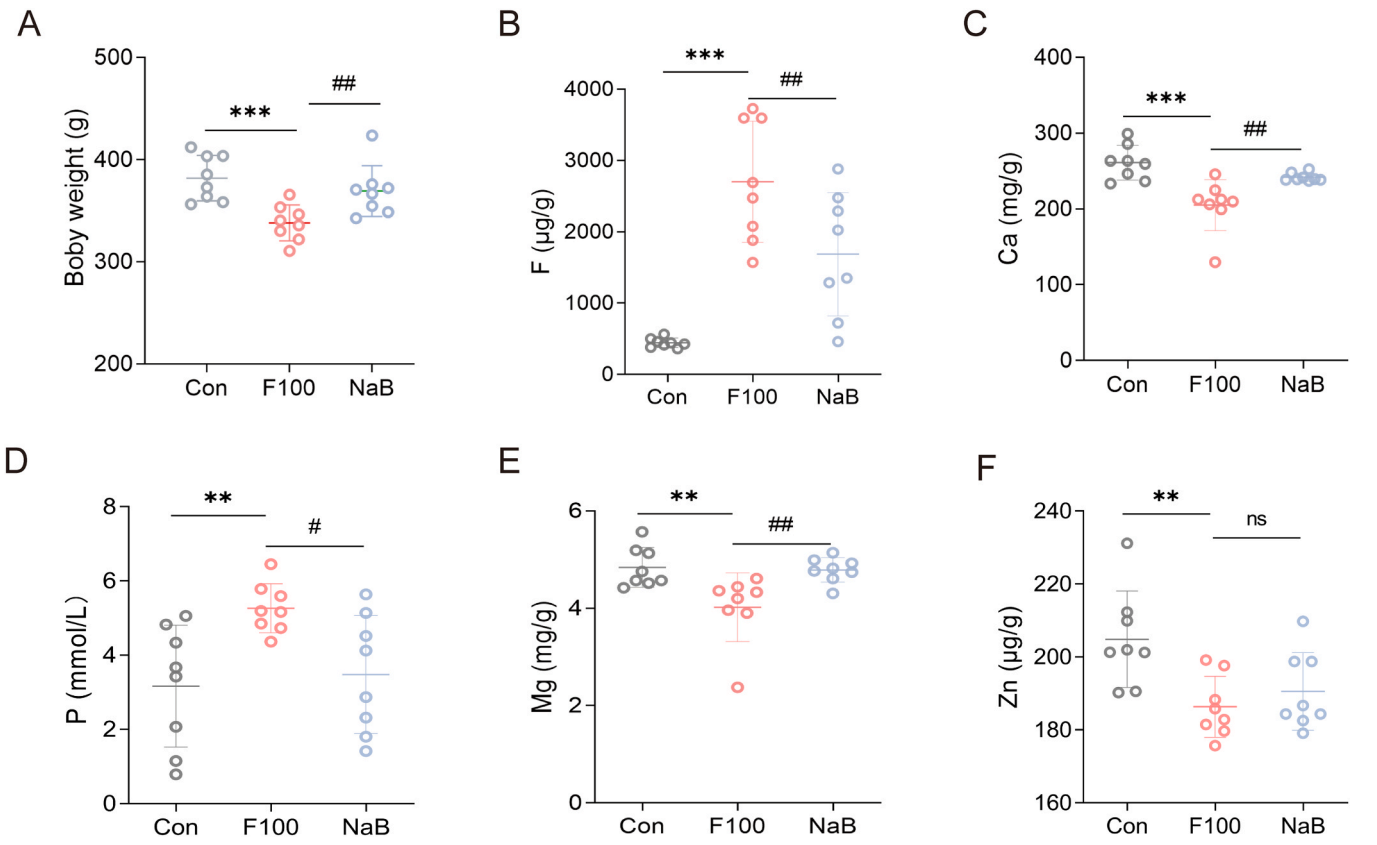

Fig. 2. Effect of NaB on final body weight and bone mineral content. (A) Final body weight of rats; (B-F) Bone mineral content in rats. B, Fluoride; C, Calcium; D, Phosphorus; E, Magnesium; F, Zinc. Error bars represent mean ± SD ($n = 8$ per group). $^{*}P < 0.05$, $^{**}P < 0.01$, $^{***}P < 0.001$ vs. the control, $^{\#}P < 0.05$, $^{\#\#}P < 0.01$, $^{\#\#\#}P < 0.001$ vs. the F100 group· F100 group (Fluorosis group at 100 mg/L NaF), and NaB group (1000 mg/kg/d NaB+100 mg/L NaF).

rate was set at 0.30 mL/min, and the injection volume for each sample was 2 μL. The mass spectrometry voltages were set to 5000 V (ESI+) and 4500 V (ESI-), and the primary scan range was 50–1200 Da. The temperature of the ion source was adjusted to 650 ℃ and the dynamic exclusion time was configured at 4 seconds.

2.7. Statistical analysis

The statistical analysis was conducted using SPSS software (version 27.0) and expressed as mean ± standard deviation (x ± s). The significance levels were denoted as $^{*}P< 0.05$, $^{**}P< 0.01$, $^{***}P < 0.001$, respectively, compared with the control group, and $^{\#}P < 0.05$, $^{\#\#}P < 0.01$, $^{\#\#\#}P < 0.001$, respectively, compared with the fluorosis group. Metabolomics original data files were normalized and converted into. CSV format using MultiQuant MD software. Principal component analysis (PCA) and Partial Least Squares Discriminant Analysis (PLS-DA) were conducted to provide an overview of the metabolic data and screen for differential metabolites. Moreover, univariate analysis was then performed using the MetaboAnalyst 5.0 platform to further compare the preliminary differential metabolites in the Kyoto Encyclopaedia of Genes and Genomes (KEGG) and Human Metabolite Database (HMDB) databases. Finally, metabolites with Variable Importance Projection (VIP) ≥ 1, $P < 0.01$, and fold change (FC) ≥ 2 or ≤ 0.5 were selected as differentially expressed metabolites with significant differences between groups, followed by identified metabolites being imported into MetaboAnalyst 5.0 (http://www.metaboanalyst.ca) and Kyoto Encyclopaedia of Genes and Genomes (KEGG; http://www.kegg.jp) for pathway analysis.

3. Results and discussion

3.1. Effects of NaB on body weight and bone mineral content

During the experiment, no mortality occurred in any of the experimental groups, and there were no significant differences observed in diet, water consumption, fur condition, or behavioral patterns among the rat groups. Nevertheless, the F100 group exhibited a statistically significant decrease in body weight compared to the Con group at the end of the experiment ($P = 0.001$; Fig. 2**A**). However, the treatment with 1000 mg/kg/day of NaB resulted in a notable increase in body weight compared to the F100 group ($P = 0.009$; Fig. 2**A**). Furthermore, the F100 group exhibited a significant reduction in bone calcium, magnesium, and zinc levels in comparison to the Con group (P = 0.001, 0.003, 0.006), while there was a considerable increase in bone fluoride and phosphorus contents (P=0.001, 0.003; Fig. 2**B-F**). Compared with the F100 group, the NaB group had increased bone calcium and magnesium (P=0.005, 0.005), whereas fluoride and phosphorus levels were decreased (P=0.005, 0.02; Fig. 2**B-F**).

In this study, a rat model of high fluoride exposure was successfully established by adding 100 mg/L NaF to the drinking water of rats. The results showed that rats exhibited impaired bone mineral metabolism under a high fluoride environment, which is consistent with previous research findings (Sharma et al., 2022). However, intervention with 1000 mg/kg/day of NaB significantly improved the bone homeostasis of fluorosis rats, as evidenced by a significant reduction in bone fluoride and phosphorus content and a significant increase in bone calcium and magnesium content. These results suggest that NaB can effectively restore the changes in body weight and bone mineral content induced by fluoride in rats.

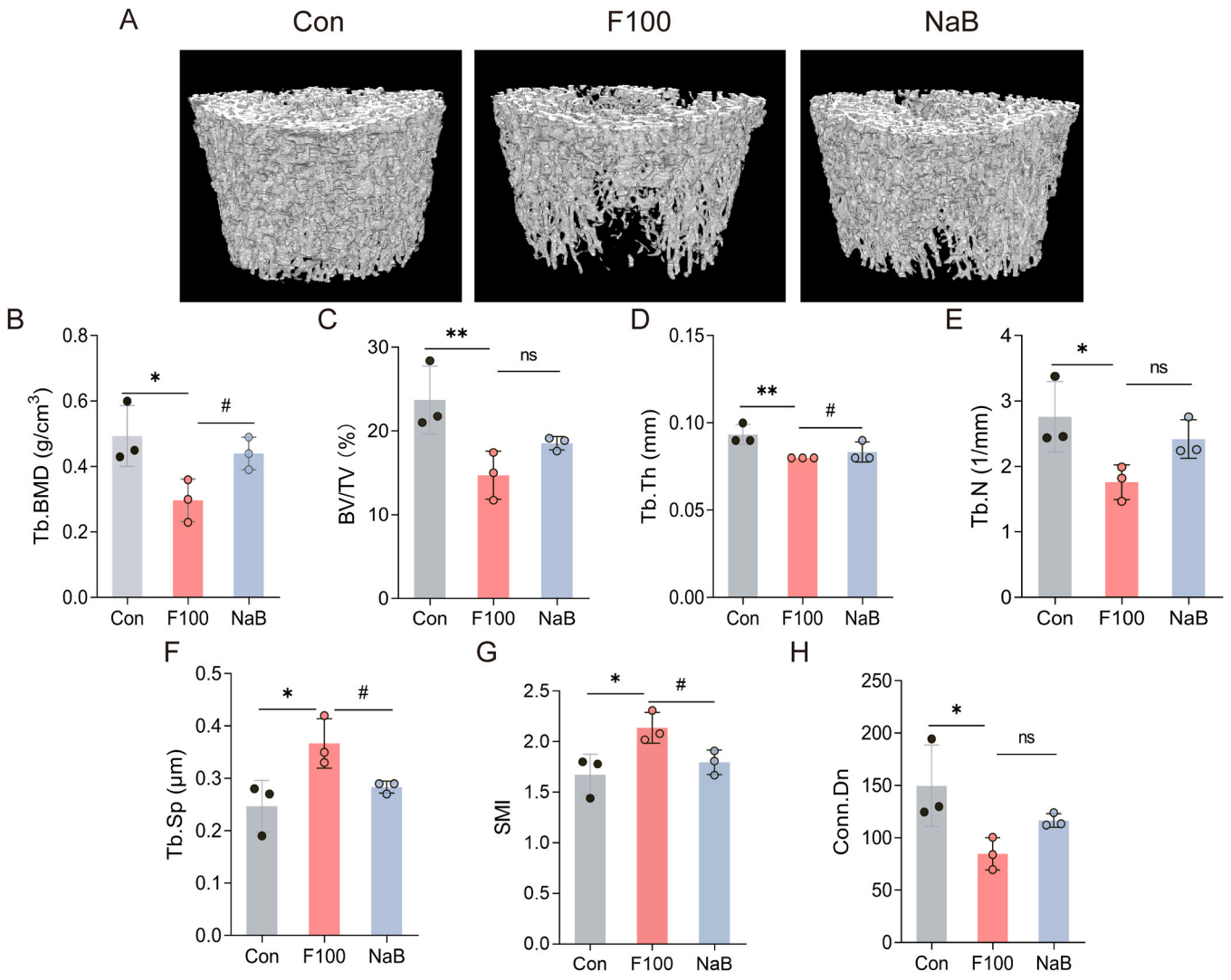

Fig. 3. Effect of NaB on femur development. (A) Three-dimensional structure of trabecular bone by micro-CT; (B) Trabecular bone mineral density (Tb. BMD); (C) Bone volume/total volume (BV/TV); (D) Trabecular thickness (Tb. th); (E) Trabecular number (Tb. N); (F) Trabecular separation (Tb. Sp); (G) Structural model index (SMI); (H) Connectivity density (Conn.Dn). Error bars represent mean ± SD ($n = 3$ per group). $^{*}P < 0.05$, $^{**}P < 0.01$, $^{***}P < 0.001$ vs. the control, $^{\#}P < 0.05$, $^{\#\#}P < 0.01$, $^{\#\#\#}P < 0.001$ vs. the F100 group.

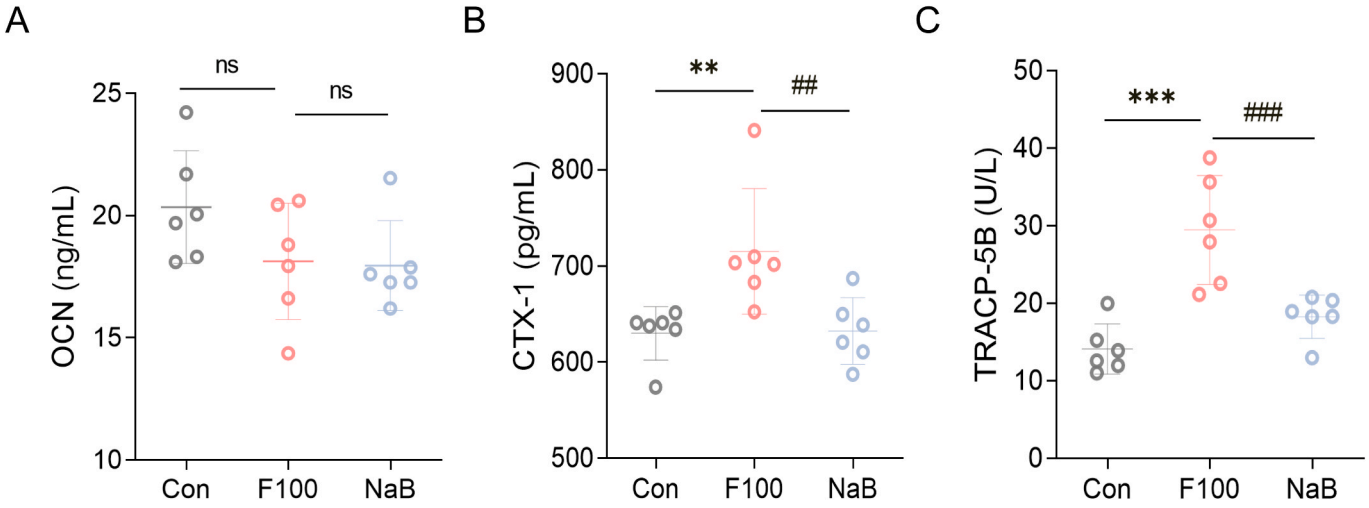

Fig. 4. Effect of NaB on plasma biochemical indicators. (A) OCN; (B) CTX-1; (C) TRACP-5B. Error bars represent mean ± SD ($n = 6$ per group). $^{*}P < 0.05$, $^{**}P < 0.01$, $^{***}P < 0.001$ vs. the control, $^{\#}P < 0.05$, $^{\#\#}P < 0.01$, $^{\#\#\#}P < 0.001$ vs. the F100 group.

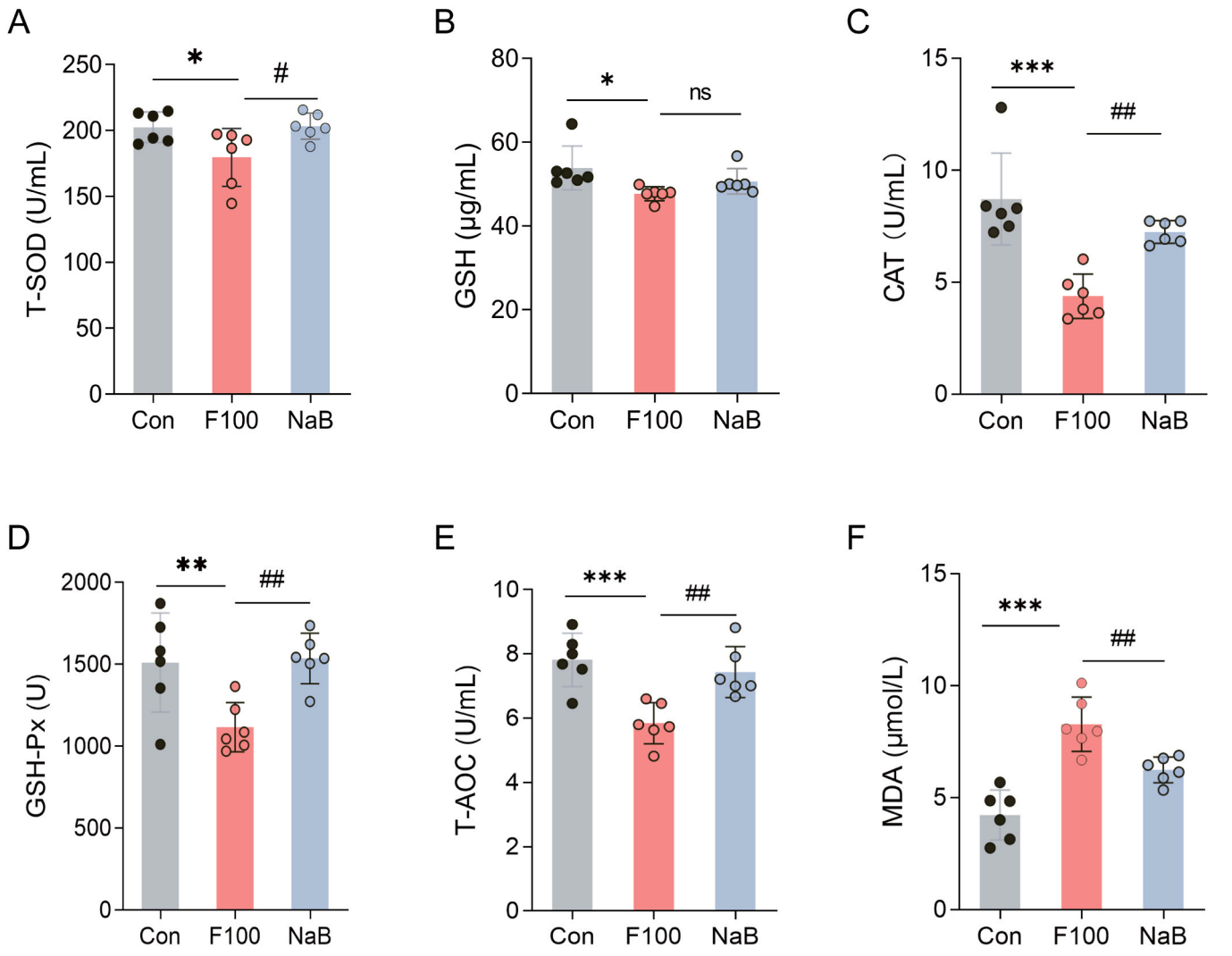

Fig. 5. Effect of NaB on oxidative stress indicators. (A) T-SOD; (B) GSH; (C) CAT; (D) GSH-Px; (E) T-AOC. Error bars represent mean ± SD. $^{*}P < 0.05$, $^{**}P < 0.01$, $^{***}P < 0.001$ vs. the control, $^{\#}P < 0.05$, $^{\#\#}P < 0.01$, $^{\#\#\#}P < 0.001$ vs. the fluorosis 100 mg/L. Error bars represent mean ± SD ($n = 6$ per group). $^{*}P < 0.05$, $^{**}P < 0.01$, $^{***}P < 0.001$ vs. the control, $^{\#}P < 0.05$, $^{\#\#}P < 0.01$, $^{\#\#\#}P < 0.001$ vs. the F100 group.

3.2. Effects of NaB on femur development

To investigate the anti-fluorosis effects of NaB treatment, we analyzed the morphology of bone trabeculae, changes in bone density, and three-dimensional structure by micro-CT. As can be seen in Fig. 3**A**, the trabecular structure of the femur in the F100 group was sparse and heterogeneous compared with the Con group and fractured and missing trabeculae were observed in the ROI region. However, compared with the F100 group, the NaB group exhibited a relatively denser trabecular structure and increased trabeculae in the ROI region. Moreover, some microstructural damages to bone were relatively less severe. It can be seen from Fig. 3**B-H** that BMD, BV/TV, Tb. Th, Tb. N, and Conn. Dn in the F100 group was significantly lower than in the Con group (P=0.01, 0.009, 0.002, 0.02, 0.02), while Tb. Sp and SMI values were significantly increased (P=0.01, 0.01). However, there was a significant increase in femoral BMD and Tb. Th in the NaB group compared to the F100 group (P=0.04, 0.04), whereas Tb. Sp and SMI values were significantly decreased (P=0.04, 0.04).

Overall, micro-CT analysis revealed abnormal femoral trabecular morphology in fluorosis rats, indicating impaired bone quality and structural characteristics, which is in accordance with the findings of Li et al.(Li et al., 2023). Nevertheless, the morphology of bone trabeculae showed a significant improvement after administering NaB. These findings suggest that NaB can effectively improve bone loss caused by fluorosis.

3.3. Effects of NaB on plasma biochemical indicators

To further investigate the regulatory effects of NaB in fluorosis rats, biomarkers related to bone formation and resorption were examined. As shown in Fig. 4**A-C**, plasma biochemical analysis indicated that the OCN levels in the F100 group showed a decreasing trend but were not statistically significant, whereas the CTX-I and TRACP-5 levels in the F100 group were significantly higher (P=0.005, 0.001) compared with the con group. Moreover, compared with the F100 group, the OCN levels in the NaB group showed a slight upward trend, while the CTX-I and TRACP-5B levels in the NaB group were significantly decreased (P=0.007, 0.001).

Bone metabolism refers to the dynamic balancing of bone formation and resorption. When bone resorption exceeds bone formation, bone loss is manifested as osteoporosis. BALP, OCN, TRACP-5B, and CTX-I are specific markers reflecting bone formation and resorption (Garnero, 2006). OCN is synthesized and secreted by osteoblasts, and its level can reflect the process of bone formation (Han et al., 2018). CTX-I, a sensitive marker for bone resorption, is associated with type I collagen, while TRACP-5B promotes bone resorption. The present study

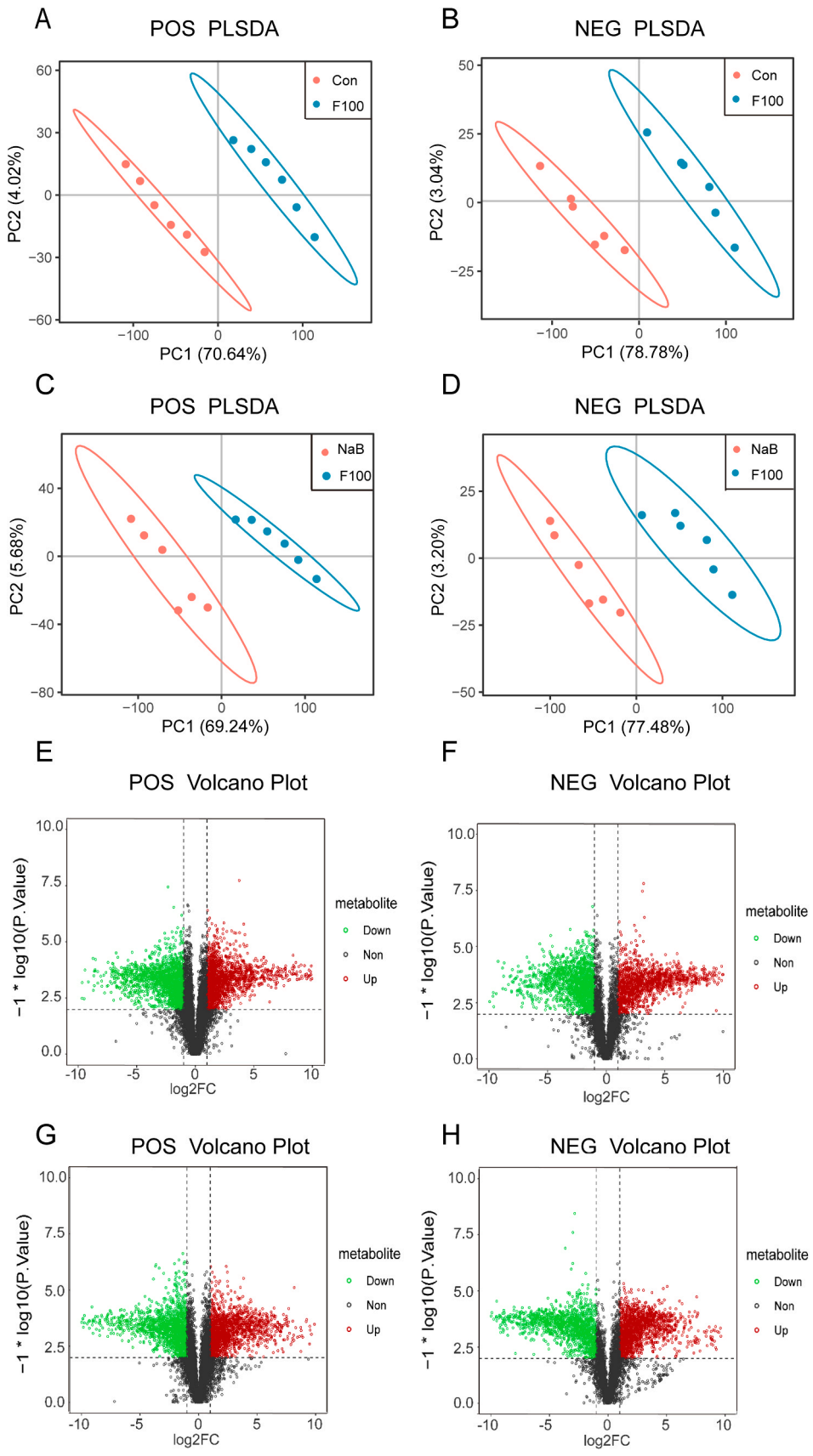

(caption on next page)

Fig. 6. Fluoride exposure altered the metabolite profile of serum contents. (A, C) Plots of PLS-DA scores of metabolic changes in serum samples for Con vs. F100 group and F100 vs. NaB group in positive ion mode, respectively, $n = 6$ per group; (B, D) Plots of PLS-DA scores of metabolic changes in serum samples for Con vs. F100 group and F100 vs. NaB group in negative ion mode, respectively; (E, G) Differential expression Volcano Plots in serum samples for Con vs. F100 group and F100 vs. NaB in positive ion mode, respectively; (F, H) Differential expression Volcano Plots in serum samples for Con vs. F100 group and F100 vs. NaB in negative ion mode, respectively.

demonstrated that 100 mg/L fluoride affected the levels of biomarkers of bone resorption thereby disrupting bone homeostasis, which is in line with Wang's findings that high fluoride levels lead to abnormal bone activity (Wang et al., 2019b). Interestingly, the above results confirmed that NaB could reverse this disturbance in bone growth and alleviate fluorosis by regulating bone resorption.

3.4. Effects of NaB on oxidative stress indicators

To clarify how NaB alleviates bone tissue damage in rats with fluorosis, we conducted a detailed analysis of its effects on oxidative stress indicators. As depicted in Fig. 5**A-F**, compared to the Con group, the F100 group exhibited a significant decrease in the levels of T-SOD, GSH, CAT, GSH-Px, and T-AOC (P=0.02, 0.01, 0.001, 0.01, 0.001), indicative of impaired antioxidant defenses. Additionally, there was a significant increase in MDA content (P=0.001), suggesting heightened oxidative damage and lipid peroxidation. In contrast, the NaB group showed significantly higher T-SOD, CAT, and T-AOC levels (P=0.02, 0.002, 0.002) and a significantly lower MDA level (P=0.003) than the F100 group.

Fluoride exposure increases the generation of reactive oxygen species (ROS) and diminishes antioxidant capacity (Srivastava and Flora, 2020b), leading to fluoride-induced oxidative stress. In the experiment, a significant decrease in serum levels of T- SOD, GSH, CAT, GSH-Px, and T-AOC was observed in fluoride-exposed rats, along with a marked increase in MDA. These findings suggested that high levels of fluoride decreased the antioxidant enzyme activity, thereby increasing MDA levels, which in turn led to oxidative stress. However, it was observed that the administration of NaB effectively alleviated the oxidative stress in rats with fluorosis. To sum up, NaB can improve antioxidant capacity and reduce lipid peroxidation and oxidative stress.

3.5. Serum metabolomics

Fluorosis-induced bone damage is a type of bone tissue metabolism disorder closely associated with changes in metabolites, but the specific metabolic features associated with it remain unclear. In order to investigate the mechanism by which NaB alleviated fluorosis in rats, LC-MS analysis of small molecule endogenous metabolites was conducted to reveal changes in the metabolic profile, thereby elucidating the potential mechanisms underlying NaB intervention in fluorosis.

The ion flow charts of the total serum and quality control samples are illustrated in **Figure S1**. The PCA score plots in **Figure S2A-B**, distinctly separated the Con and F100 groups, demonstrating clear clustering, which was also observed between the F100 and NaB groups (**Figure S2C-D)**. Further analysis with PLS-DA, revealed the model's stability and predictability through the evaluation parameters R^2 and Q^2 (**Figure S2E-H**). This analysis revealed significant clustering in both ion modes for the Con vs. F100 group comparison, indicating a deviation from normal metabolic levels in the F100 group due to fluorosis. Similarly, clear clustering between the F100 vs. NaB groups indicates that NaB treatment potentially counteracts the metabolic changes induced by fluorosis, as shown in Fig. 6**A-D**.

Volcano plots were employed as a screening tool for identifying differential metabolites. In both positive ion mode **(**Fig. 6**E)** and negative ion mode **(**Fig. 6**F)**, 1689 and 1487 metabolites were up-regulated, and 1712 and 1614 metabolites were down-regulated in the F100 group compared with the Con group, respectively. Comparatively, in the positive ion mode **(**Fig. 6**G)**, the NaB group up-regulated 1650 metabolites and down-regulated 1557 metabolites, whereas, in the negative ion mode **(**Fig. 6**H)**, the NaB group up-regulated 1517 metabolites and down-regulated 1440 metabolites, respectively.

For deeper metabolic pathway analysis, we selected metabolites based on variables with VIP $\geq$ 1 and FC $\geq$ 2 or $\leq$ 0.5 with P $<$ 0.01. By comparing the data between the Con vs. F100 and F100 vs. NaB groups, a total of 1438 and 1542 differentially expressed metabolites were identified, respectively. Subsequently, KEGG metabolic pathways were used to analyze the potential metabolic pathways of NaB for alleviating fluorosis. As shown in Fig. 7**A-B**, larger log(p) values and redder colors indicate higher importance of the metabolite and more significant effects, indicating the involvement of more nodes affected by the metabolite. Pathways with impact values $>$ 0.1 and -log10(p) values $>$1.0 were considered to be significantly affected metabolic pathways. The results showed that fluorosis may be related to arginine and proline metabolism and glycerophospholipid metabolism, consistent with previous research (Zhao et al., 2022b) (Yue et al., 2020). Arachidonic acid metabolism, steroid hormone biosynthesis, and arginine and proline metabolism were found to be the most important pathways involved in the prevention of fluorosis by NaB. In these comparative groups, there is a certain degree of overlap between the pathways of arginine and proline metabolism. This suggests that NaB may affect this metabolic pathway and be associated with these seven biomarkers (Fig. 7**C-D**) to antagonize fluorosis. A detailed analysis of the metabolic pathways and associated metabolites can be found in Table 1 and **Table S1–2**.

Metabolomics analysis of rat serum revealed significant deviations in the metabolite profile of fluorosis rats, indicating metabolic disturbances. NaB treatment shifted the metabolite profiles towards normal levels, indicating its antagonistic effect on fluorosis-related metabolic changes. Further analysis revealed that NaF primarily affected pathways associated with arginine and proline metabolism and glycerophospholipid metabolism, whereas NaB mainly influenced pathways related to arachidonic acid metabolism, arginine and proline metabolism, and steroid hormone biosynthesis. Obviously, arginine and proline metabolism emerged as a shared pathway, suggesting its crucial role in the NaB treatment of fluorosis. After NaB intervention in fluorosis rats, several metabolites in arginine and proline metabolism showed significant changes, including 1-Pyrroline-4-hydroxy-2-carboxylate, 4-Hydroxyproline, cis-4-Hydroxy-D-proline, L-1-Pyrroline-3-hydroxy-5-carboxylate, L-Glutamic gamma-semialdehyde, S-Adenosylmethionine, 4-Hydroxyproline, and Trans-3 hydroxy-L-proline.

Previous research has linked arginine and proline metabolism to protecting against bone loss (Onuora, 2023). In this study, we observed a significant increase in the blood metabolites 1-pyrroline-4-hydroxy-2--carboxylate and L-1-pyrroline-3-hydroxy-5-carboxylate, which are intermediate products in the arginine synthesis pathway and can be converted to arginine by arginine synthase. This finding is consistent with recent studies showing increased arginine biosynthesis in saliva samples of dental fluorosis patients (Liu et al., 2023a). Arginine and proline play a crucial role in protecting against oxidative stress by maintaining intracellular redox homeostasis and increasing catalase activity (Lin et al., 2005; Zhang et al., 2015). Proline has been found to regulate oxidative metabolism during osteoblast development and serve as a source of energy. In the case of fluorosis, proline contributes to the production of additional ATP to meet the increased energy demands of cells caused by oxidative stress (Phang et al., 2008). These findings suggest a potential link between fluoride exposure and oxidative stress. Further research is needed to explore the specific mechanisms involved in arginine and proline biosynthesis in response to oxidative damage.

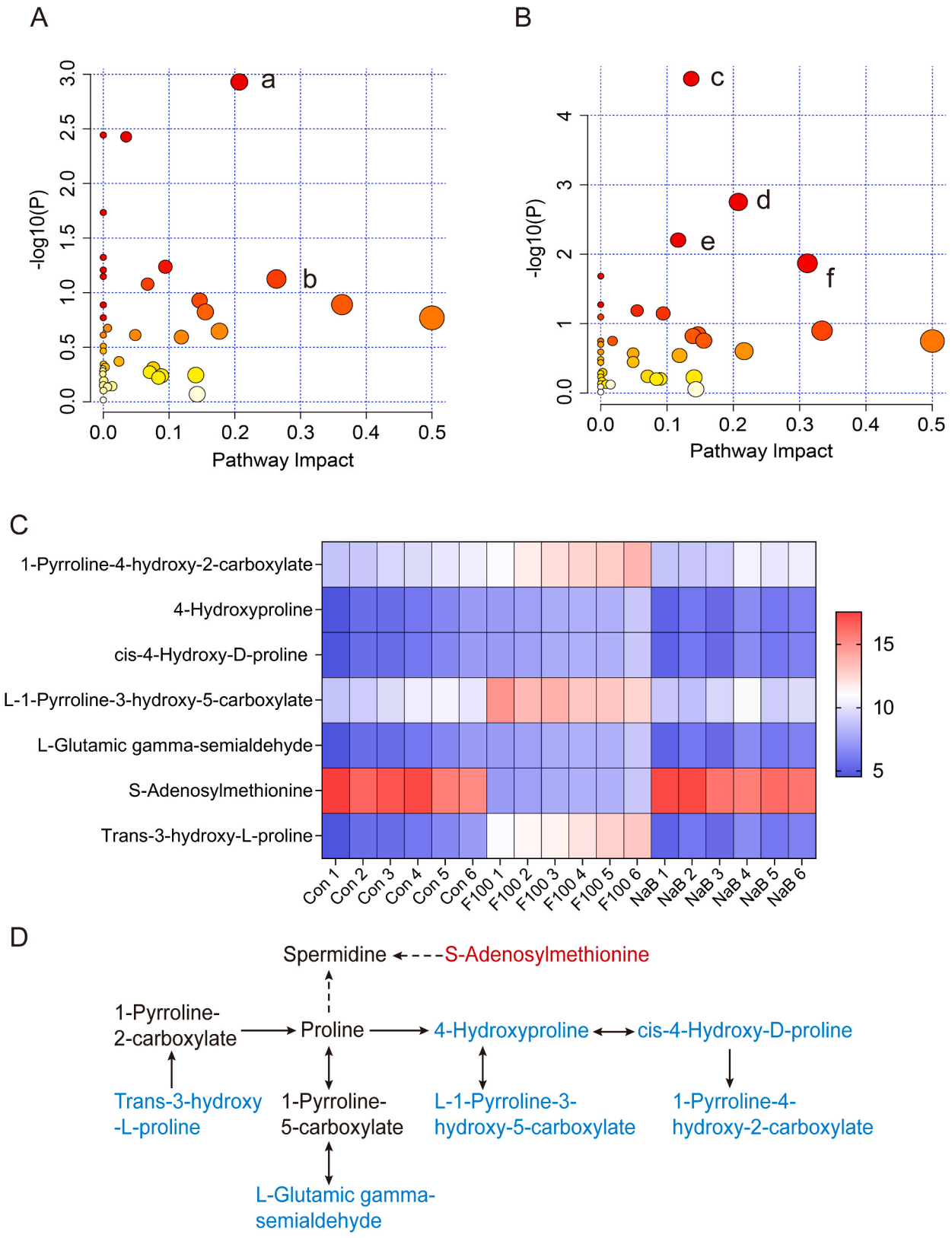

Fig. 7. Overview of the key differential metabolites and related metabolic pathways. (A) Metabolic pathways involved in all markers in serum for fluoride exposure. a, Arginine and proline metabolism; b, Glycerophospholipid metabolism. (B) Metabolic pathways involved in all markers in serum regulated by NaB. c, Arachidonic acid metabolism; d, Steroid hormone biosynthesis; e, Arginine and proline metabolism; f, Citrate cycle (TCA cycle). The size and color of each circle are based on the pathway impact value and p value, respectively. (C) Heatmap for the effect of NaB treatment on arginine and proline metabolism pathway in fluorosis rats, $n = 6$ per group. (D) The metabolic profiles altered after NaB treatment analyzed by the KEGG database. Red highlights in the metabolic pathway indicate up-regulated metabolic profiles, while blue highlights indicate down-regulated metabolic profiles.

Table 1
Potential biomarkers associated with NaB treatment in rat serum in the metabolic pathway.

No	Metabolite	MODE	Formula	Kegg ID	Fold change Con vs F100	F100 vs NaB	Trend Con vs F100	F100 vs NaB
1	1-Pyrroline-4-hydroxy-2-carboxylate	+	C5H7NO3	C04282	6.74	0.14	↑***	↓***
2	4-Hydroxyproline	+	C5H9NO3	C01157	5.39	0.2	↑***	↓***
3	cis-4-Hydroxy-D-proline	+	C5H9NO3	C03440	4	0.24	↑***	↓***
4	L-1-Pyrroline-3-hydroxy-5-carboxylate	+	C5H7NO3	C04281	4	0.24	↑***	↓***
5	L-Glutamic gamma-semialdehyde	+	C5H9NO3	C01165	4	0.24	↑***	↓***
6	S-Adenosylmethionine	-	C15H23N6O5S	C00019	0.12	7.04	↓**	↑**
7	Trans-3-hydroxy-L-proline	+	C5H9NO3	C05147	4	0.24	↑***	↓***

[a]Fold change equals the fold difference in concentration observed between two groups. ↑: upregulated. ↓: downregulated. *$P < 0.05$, **$P < 0.01$, ***$P < 0.001$.

S-adenosylmethionine (SAM) is an essential substance in the arginine synthesis pathway, contributing to DNA and protein synthesis in bone cells and playing a critical regulatory role in bone formation. Previous studies have shown that high levels of SAM increase the risk of fragility fractures and osteoporosis (McLean et al., 2004; Van Meurs et al., 2004). During osteoclast differentiation, the oxidative metabolism of the cells tends to increase, meaning that they become more reliant on oxidative pathways to generate energy, accompanied by an increase in SAM levels (Nishikawa et al., 2015). Increases in serum collagen cross-linked peptides (CTX) and TRACP-5B positively correlate with enhanced osteoclast activity and increased systemic bone resorption (Rissanen et al., 2008; Both et al., 2018). Conversely, serum osteocalcin (OCN) content is negatively correlated with enhanced osteoclast activity and increased systemic bone resorption, as confirmed by our findings (Liu et al., 2023b). Herman's study suggested that SAM-induced tissue-specific accumulation of homocysteine in bone by binding to collagen, accompanied by bone loss and decreased bone strength. This may be related to the pathological mechanism of decreased methylation capacity of osteoblasts (Herrmann et al., 2009). Therefore, we speculate that SAM may be involved in the intracellular methylation reactions in NaB group rats by providing methyl groups, regulating redox balance, and ameliorating the pathological mechanisms of fluorosis.

Fluorosis is a bone metabolism disorder due to excessive fluoride intake. Our study found increased serum levels of 4-hydroxyproline, cis-4-hydroxy-D-proline, and trans-3-hydroxy-L-proline, consistent with previous findings (Zhao et al., 2022). Proline is an essential amino acid involved in collagen synthesis, which plays a crucial role in maintaining the structure and strength of connective tissues like bones and cartilage (Li and Wu, 2018; Karna et al., 2020). Disrupted proline metabolism may affect collagen production and, thus, bone tissue structure, suggesting a potential mechanism for fluorosis development. Hydroxyproline is produced by proline hydroxylation within the peptide chain by prolyl hydroxylase. Collagenases can break down collagen, releasing hydroxyproline into the bloodstream and increasing its concentration (Wu et al., 2019). The increased serum hydroxyproline levels observed in fluorosis rats may indicate increased collagen breakdown, enhanced bone resorption, and degradation of bone tissue, which are associated with fluoride-induced bone damage. In the case of fluorosis, hydroxyproline can transfer the redox potential of the pentose phosphate pathway to the mitochondria via the proline cycle, which helps generate additional ATP to provide cells with the energy needed to cope with metabolic changes induced by oxidative stress (Phang et al., 2008). In brief, the NaB intervention restored the levels of bone homeostasis indicators and the levels of the above serum metabolites, indicating NaB may prevent fluorosis in rats by regulating bone homeostasis and serum metabolism.

Moreover, NaB affects metabolites in various metabolic pathways, such as arachidonic acid metabolism and steroid hormone biosynthesis. However, the analysis of metabolic pathways suggests that the impact of metabolites on these pathways is relatively weaker compared to arginine and proline metabolism. This could be attributed to the relatively lower importance of these metabolites within their respective pathways. Arginine and proline metabolism primarily contribute to osteoblast differentiation and synthesis, potentially improving bone mass and skeletal structure by mitigating oxidative stress. Nevertheless, the up- or down-regulation of differential metabolites analyzed using LC-MS in the present study is a relative change, and quantification of key differential metabolites in serum metabolism is necessary for future studies to determine in depth the potential mechanisms by which NaB regulates bone homeostasis and serum metabolism.

Altogether, our study demonstrates the protective effect of NaB against fluorosis in rats by modulating bone homeostasis and serum metabolism, which corroborates previous findings that SCFA significantly modulates the development of skeletal and bone metabolism-related diseases (Lucas et al., 2018b; Montalvany-Antonucci et al., 2019). Although clinical studies of butyrate have shown results that are much more complex than experimental models, there is some evidence to support a protective role for butyrate in disease (Patz et al., 1996; Luceri et al., 2016; Elfadil et al., 2023). However, direct supplementation with butyrate differs from endogenous butyrate production, which is combined with circadian rhythmic fermentation (Leone et al., 2015; Kaczmarek et al., 2017). Therefore, forms of supplementation that match physiologic patterns are promoted for the future (Sobh et al., 2022; Hodgkinson et al., 2023). It is also important to note that exogenously administered NaB interferes with the patient's own butyrate metabolism and it remains to be demonstrated whether the health benefits conferred derive solely from the presence of butyrate. Future promising clinical studies are therefore necessary to elucidate in depth the role of butyrate in various diseases.

4. Conclusion

In this study, we have demonstrated that NaB effectively improves bone homeostasis in rats affected by fluorosis. Specifically, NaB treatment increased bone mineral density and content, improved bone tissue morphology and microstructure, modulated bone resorption, and reduced oxidative stress. Furthermore, this research offers a novel perspective through serum metabolomics, showing that NaB treatment alters the endogenous metabolic profile in fluorosis rats. Key metabolic pathways, particularly those involving metabolites such as 1-Pyrroline-4-hydroxy-2-carboxylate and 4-Hydroxyproline, which play a role in arginine and proline metabolism, emerge as primary characteristics of the metabolic profile post-NaB treatment. In conclusion, this study deepens our understanding of NaF toxicity mechanisms and sheds light on the metabolic profile after NaB treatment. Furthermore, it contributes to identifying potential biomarkers for fluorosis, developing intervention strategies, and paving the way for new therapeutic approaches to treating fluorosis.

Ethics approval

Our study was conducted according to the tenets of the Declaration of Helsinki. The animal experiments were reviewed and approved by the Laboratory Animal Ethics Committee of Shenyang Medical College (No. SYYXY2019040602).

CRediT authorship contribution statement

Ying Li: Writing – original draft, Visualization, Software, Methodology, Data curation. **Fengmei Yang:** Writing – original draft, Visualization, Software, Methodology, Data curation. **Jie Liu:** Writing – original draft, Visualization, Software, Methodology, Data curation. **Mengqi Jiang:** Validation, Data curation. **Zhuo Zhang:** Writing – review & editing, Writing – original draft, Validation, Supervision, Project administration, Methodology, Conceptualization. **Lin Zhou:** Writing – review & editing, Writing – original draft, Visualization, Supervision, Software, Project administration, Methodology, Conceptualization. **Lu Sun:** Writing – review & editing, Writing – original draft, Validation, Project administration, Methodology, Conceptualization. **Ye Yu:** Validation, Data curation. **Qingyi Zhou:** Data curation.

Declaration of Competing Interest

The authors declare that they have no known competing financial interests or personal relationships that could have appeared to influence the work reported in this paper.

Data Availability

Data will be made available on request.

Acknowledgments

This research was supported by Postgraduate Scientific Research Innovation Project of Shenyang Medical College (Y20220520) and the Natural Science Foundation of Liaoning Province of China (2021-MS-352). The authors thank to BioRender.com for providing material to draw the experimental schedule.

Appendix A. Supporting information

Supplementary data associated with this article can be found in the online version at doi:10.1016/j.ecoenv.2024.116284.

References

Babu, S., Manoharan, S., Ottappilakkil, H., Perumal, E., 2022. Role of oxidative stress-mediated cell death and signaling pathways in experimental fluorosis. Chem. -Biol. Inter. 365 https://doi.org/10.1016/j.cbi.2022.110106.

Both, T., Zillikens, M.C., Schreuders-Koedam, M., Vis, M., Lam, W.-K., Weel, A.E.A.M., van Leeuwen, J.P.T.M., van Hagen, P.M., van der Eerden, B.C.J., van Daele, P.L.A., 2018. Hydroxychloroquine affects bone resorption both in vitro and in vivo. J. Cell Physiol. 233, 1424–1433. https://doi.org/10.1002/jcp.26028.

Chen, P.S., Toribara, T.Y., Warner, H., 1956. Microdetermination of phosphorus. Anal. Chem. 28, 1756–1758. https://doi.org/10.1021/ac60119a033.

Collins, M.T., Marcucci, G., Anders, H.-J., Beltrami, G., Cauley, J.A., Ebeling, P.R., Kumar, R., Linglart, A., Sangiorgi, L., Towler, D.A., Weston, R., Whyte, M.P., Brandi, M.L., Clarke, B., Thakker, R.V., 2022. Skeletal and extraskeletal disorders of biomineralization. Nat. Rev. Endocrinol. 18, 473–489. https://doi.org/10.1038/s41574-022-00682-7.

Egorin, M.J., Yuan, Z.M., Sentz, D.L., Plaisance, K., Eiseman, J.L., 1999. Plasma pharmacokinetics of butyrate after intravenous administration of sodium butyrate or oral administration of tributyrin or sodium butyrate to mice and rats. Cancer Chemother. Pharm. 43, 445–453. https://doi.org/10.1007/s002800050922.

Elfadil, O.M., Mundi, M.S., Abdelmagid, M.G., Patel, A., Patel, N., Martindale, R., 2023. Butyrate: More Than a Short Chain Fatty Acid. Curr. Nutr. Rep. 12, 255–262. https://doi.org/10.1007/s13668-023-00461-4.

Garcia, A.L.H., Picinini, J., Silveira, M.D., Camassola, M., Visentim, A.P.V., Salvador, M., da Silva, J., 2021. Fluorosilicic acid induces DNA damage and oxidative stress in bone marrow mesenchymal stem cells (https://doi.org/). Mutat. Res-Gen. Tox Environ. 861. https://doi.org/10.1016/j.mrgentox.2020.503297.

Garnero, P., 2006. Chapter 10 - Biochemical markers of bone turnover. In: Lane, N.E., Sambrook, P.N. (Eds.), Osteopor Osteopor Rheumat Dis. Mosby, Philadelphia, pp. 88–99. https://doi.org/10.1016/B978-0-323-03437-1.50017-8.

Han, Y.J., You, X.L., Xing, W.H., Zhang, Z., Zou, W.G., 2018. Paracrine and endocrine actions of bone-the functions of secretory proteins from osteoblasts, osteocytes, and osteoclasts. Bone Res 6. https://doi.org/10.1038/s41413-018-0019-6.

Herrmann, M., Tami, A., Wildemann, B., Wolny, M., Wagner, A., Schorr, H., Taban-Shomal, O., Umanskaya, N., Ross, S., Garcia, P., Hübner, U., Herrmann, W., 2009. Hyperhomocysteinemia induces a tissue specific accumulation of homocysteine in bone by collagen binding and adversely affects bone. Bone 44, 467–475. https://doi.org/10.1016/j.bone.2008.10.051.

Hodgkinson, K., El Abbar, F., Dobranowski, P., Manoogian, J., Butcher, J., Figeys, D., Mack, D., Stintzi, A., 2023. Butyrate`s role in human health and the current progress towards its clinical application to treat gastrointestinal disease. CLIN NUTR 42, 61–75. https://doi.org/10.1016/j.clnu.2022.10.024.

Iwami, K., Moriyama, T., 1993. Effects of short-chain fatty-acid, sodium-butyrate, on osteoblastic cells and osteoclastic cells. Int J. Biochem 25, 1631–1635. https://doi.org/10.1016/0020-711X(93)90522-G.

Jin, Y., Zhou, B.-H., Zhao, J., Ommati, M.M., Wang, S., Wang, H.-W., 2023. Fluoride-induced osteoporosis via interfering with the RANKL/RANK/OPG pathway in ovariectomized rats: oophorectomy shifted skeletal fluorosis from osteosclerosis to osteoporosis. Environ. Pollut. 336, 122407 https://doi.org/10.1016/j.envpol.2023.122407.

Kaczmarek, J.L., Musaad, S.M.A., Holscher, H.D., 2017. Time of day and eating behaviors are associated with the composition and function of the human gastrointestinal microbiota. Am. J. Clin. Nutr. 106, 1220–1231. https://doi.org/10.3945/ajcn.117.156380.

Karna, E., Szoka, L., Huynh, T.Y.L., Palka, J.A., 2020. Proline-dependent regulation of collagen metabolism. Cell Mol. Life Sci. 77, 1911–1918. https://doi.org/10.1007/s00018-019-03363-3.

Katono, T., Kawato, T., Tanabe, N., Suzuki, N., Iida, T., Morozumi, A., Ochiai, K., Maeno, M., 2008. Sodium butyrate stimulates mineralized nodule formation and osteoprotegerin expression by human osteoblasts. Arch. Oral. Biol. 53, 903–909. https://doi.org/10.1016/j.archoralbio.2008.02.016.

Khan, S., Jena, G., 2016. Sodium butyrate reduces insulin-resistance, fat accumulation and dyslipidemia in type-2 diabetic rat: a comparative study with metformin. Chem. Biol. Interact. 254, 124–134. https://doi.org/10.1016/j.cbi.2016.06.007.

Leone, V., Gibbons, S.M., Martinez, K., Hutchison, A.L., Huang, E.Y., Cham, C.M., Pierre, J.F., Heneghan, A.F., Nadimpalli, A., Hubert, N., Zale, E., Wang, Y.W., Huang, Y., Theriault, B., Dinner, A.R., Musch, M.W., Kudsk, K.A., Prendergast, B.J., Gilbert, J.A., Chang, E.B., 2015. Effects of diurnal variation of gut microbes and high-fat feeding on host circadian clock function and metabolism. Cell Host Microbe 17, 681–689. https://doi.org/10.1016/j.chom.2015.03.006.

Li, B., Wang, Y., Gong, S., Yao, W., Gao, H., Liu, M., Wei, M., 2022. Puerarin improves OVX-induced osteoporosis by regulating phospholipid metabolism and biosynthesis of unsaturated fatty acids based on serum metabolomics. Phytomedicine 102, 154198. https://doi.org/10.1016/j.phymed.2022.154198.

Li, H.Y., Chen, X.X., Zhang, Z.H., Zhang, J.M., Xu, H., 2023. Microstructural analysis of cancellous bone in fluorosis rats. Biol. Trace Elem. Res. 201, 4827–4833. https://doi.org/10.1007/s12011-023-03564-9.

Li, P., Wu, G., 2018. Roles of dietary glycine, proline, and hydroxyproline in collagen synthesis and animal growth. Amino Acids 50, 29–38. https://doi.org/10.1007/s00726-017-2490-6.

Lin, W.T., Yang, S.C., Chen, K.T., Huang, C.C., Lee, N.Y., 2005. Protective effects of arginine on pulmonary oxidative stress and antioxidant defenses during exhaustive exercise in rats. Acta Pharm. Sin. 26, 992–999. https://doi.org/10.1111/j.1745-7254.2005.00155.x.

Liu, H., Zhang, J.J., Li, X., Yang, Y., Xie, X.F., Hu, K., 2015. Post-occlusion administration of sodium butyrate attenuates cognitive impairment in a rat model of chronic cerebral hypoperfusion. Pharmacol. Biochem. Be 135, 53–59. https://doi.org/10.1016/j.pbb.2015.05.012.

Liu, S.S., Song, Q.S., Zhang, C.C., Li, M.W., Li, Z.Z., Liu, Y.D., Xu, L., Xie, X.F., Zhao, L.L., Zhang, R.X., Wang, Q.L., Zeng, G.J., Zhang, Y.F., Zhang, K., 2023a. Saliva microbiome alterations in dental fluorosis population. J. Oral. Microbiol 15. https://doi.org/10.1080/20002297.2023.2180927.

Liu, X.L., Zhang, C.J., Shi, J.J., Ke, Q.F., Ge, Y.W., Zhu, Z.A., Guo, Y.P., 2023b. Nacre-mimetic cerium-doped nano-hydroxyapatite/chitosan layered composite scaffolds regulate bone regeneration via OPG/RANKL signaling pathway. J. Nanobiotechnol. 21 https://doi.org/10.1186/s12951-023-01988-y.

Liu, Z., Yao, X., Jiang, W., Zhou, Z., Yang, M., 2023c. Sodium butyrate enhances titanium nail osseointegration in ovariectomized rats by inhibiting the PKCα/NOX4/ROS/NF-κB pathways. J. Orthop. Surg. Res 18, 556. https://doi.org/10.1186/s13018-023-04013-y.

Liu, Z.Y., Yao, X.W., Jiang, W.K., Zhou, Z., Yang, M., 2023d. Sodium butyrate enhances titanium nail osseointegration in ovariectomized rats by inhibiting the PKCα/NOX4/ROS/NF-κB pathways. J. Orthop. Surg. Res. 18 https://doi.org/10.1186/s13018-023-04013-y.

Lucas, S., Omata, Y., Hofmann, J., Böttcher, M., Iljazovic, A., Sarter, K., Albrecht, O., Schulz, O., Krishnacoumar, B., Krönke, G., Herrmann, M., Mougiakakos, D., Strowig, T., Schett, G., Zaiss, M.M., 2018a. Short-chain fatty acids regulate systemic bone mass and protect from pathological bone loss. Nat. Commun. 9, 55. https://doi.org/10.1038/s41467-017-02490-4.

Lucas, S., Omata, Y., Hofmann, J., Böttcher, M., Iljazovic, A., Sarter, K., Albrecht, O., Schulz, O., Krishnacoumar, B., Krönke, G., Herrmann, M., Mougiakakos, D., Strowig, T., Schett, G., Zaiss, M.M., 2018b. Short-chain fatty acids regulate systemic bone mass and protect from pathological bone loss. Nat. Commun. 9 https://doi.org/10.1038/s41467-017-02490-4.

Luceri, C., Femia, A.P., Fazi, M., Di Martino, C., Zolfanelli, F., Dolara, P., Tonelli, F., 2016. Effect of butyrate enemas on gene expression profiles and endoscopic/histopathological scores of diverted colorectal mucosa: a randomized trial. Dig. Liver Dis. 48, 27–33. https://doi.org/10.1016/j.dld.2015.09.005.

Martínez-Mier, E.A., Cury, J.A., Heilman, J.R., Katz, B.P., Levy, S.M., Li, Y., Maguire, A., Margineda, J., O'Mullane, D., Phantumvanit, R., Soto-Rojas, A.E., Stookey, G.K., Villa, A., Wefel, J.S., Whelton, H., Whitford, G.M., Zero, D.T., Zhang, W., Zohouri, V., 2011. Development of gold standard ion-selective electrode-based

methods for fluoride analysis. Caries Res. 45, 3–12. https://doi.org/10.1159/000321657.
McLean, R.R., Jacques, P.F., Selhub, J., Tucker, K.L., Samelson, E.J., Broe, K.E., Hannan, M.T., Cupples, L.A., Kiel, D.P., 2004. Homocysteine as a predictive factor for hip fracture in older persons. NEJM 350, 2042–2049. https://doi.org/10.1056/NEJMoa032739.
Montalvany-Antonucci, C.C., Duffles, L.F., de Arruda, J.A.A., Zicker, M.C., de Oliveira, S., Macari, S., Garlet, G.P., Madeira, M.F.M., Fukada, S.Y., Andrade, I., Teixeira, M.M., Mackay, C., Vieira, A.T., Vinolo, M.A., Silva, T.A., 2019. Short-chain fatty acids and FFAR2 as suppressors of bone resorption. Bone 125, 112–121. https://doi.org/10.1016/j.bone.2019.05.016.
Nishikawa, K., Iwamoto, Y., Kobayashi, Y., Katsuoka, F., Kawaguchi, S., Tsujita, T., Nakamura, T., Kato, S., Yamamoto, M., Takayanagi, H., Ishii, M., 2015. DNA methyltransferase 3a regulates osteoclast differentiation by coupling to an S-adenosylmethionine-producing metabolic pathway. Nat. Med. 21, 281. https://doi.org/10.1038/nm.3774.
Onuora, S., 2023. l-arginine inhibits arthritis and bone loss by reprogramming osteoclast metabolism, 760-760. https://doi.org/ Nat. Rev. Rheuma 19. https://doi.org/10.1038/s41584-023-01055-8.
Patz, J., Jacobsohn, W.Z., GottschalkSabag, S., Zeides, S., Braverman, D.Z., 1996. Treatment of refractory distal ulcerative colitis with short chain fatty acid enemas. Am J. Gastroenterol. 91, 731–734.
Phang, J.M., Pandhare, J., Liu, Y., 2008. The metabolism of proline as microenvironmental stress substrate123. J. Nutr. 138, 2008S–2015S. https://doi.org/10.1093/jn/138.10.2008S.
Podgorski, J., Berg, M., 2022. Global analysis and prediction of fluoride in groundwater. Nat. Commun. 13, 4232. https://doi.org/10.1038/s41467-022-31940-x.
Rissanen, J.P., Suominen, M.I., Peng, Z., Halleen, J.M., 2008. Secreted tartrate-resistant acid phosphatase 5b is a marker of osteoclast number in human osteoclast cultures and the rat ovariectomy model. Calcif. Tissue Int 82, 108–115. https://doi.org/10.1007/s00223-007-9091-4.
Ščančar, J., Milačič, R., Benedik, M., Bukovec, P., 2000. Determination of trace elements and calcium in bone of the human iliac crest by atomic absorption spectrometry. Clin. Chim. Acta 293, 187–197. https://doi.org/10.1016/S0009-8981(99)00239-9.
Shashi, A., Thakur, S., 2022. Gene expression and alterations of antioxidant enzymes in spleen of rats exposed to fluoride. J. Trace Elem. Med Biol. 72 https://doi.org/10.1016/j.jtemb.2022.126966.
Sobh, M., Montroy, J., Daham, Z., Sibbald, S., Lalu, M., Stintzi, A., Mack, D., Fergusson, D.A., 2022. Tolerability and SCFA production after resistant starch supplementation in humans: a systematic review of randomized controlled studies. Am. J. Clin. Nutr. 115, 608–618. https://doi.org/10.1093/ajcn/nqab402.
Srivastava, S., Flora, S.J.S., 2020b. Fluoride in Drinking Water and Skeletal Fluorosis: a Review of the Global Impact. Curr. Environ. Health Rep. 7, 140–146. https://doi.org/10.1007/s40572-020-00270-9.
Srivastava, S., Flora, S.J.S., 2020a. Fluoride in Drinking Water and Skeletal Fluorosis: a Review of the Global Impact. Curr. Environ. Health Rep. 7, 140–146. https://doi.org/10.1007/s40572-020-00270-9.
Tang, X., Ma, S.H., Li, Y.R., Sun, Y.J., Zhang, K., Zhou, Q., Yu, R.Q., 2020a. Evaluating the activity of sodium butyrate to prevent osteoporosis in rats by promoting osteal GSK-3β/Nrf2 signaling and mitochondrial function. J. Agric. Food Chem. 68, 6588–6603. https://doi.org/10.1021/acs.jafc.0c01820.
Tang, X., Ma, S.H., Li, Y.R., Sun, Y.J., Zhang, K., Zhou, Q., Yu, R.Q., 2020b. Evaluating the activity of sodium butyrate to prevent osteoporosis in rats by promoting osteal GSK-3β/Nrf2 signaling and mitochondrial function. J. Agric. Food Chem. 68, 6588–6603. https://doi.org/10.1021/acs.jafc.0c01820.
Van Meurs, J.B., Dhonukshe-Rutten, R.A., Pluijm, S.M., Van Der Klift, M., De Jonge, R., Lindemans, J., De Groot, L.C., Hofman, A., Witteman, J.C., Van Leeuwen, J.P., Breteler, M.M., Lips, P., Pols, H.A., Uitterlinden, A.G., 2004. Homocysteine levels and the risk of osteoporotic fracture. NEJM 350, 2033–2041. https://doi.org/10.1056/NEJMoa032546.
Wang, J., Yan, D., Zhao, A., Hou, X., Zheng, X., Chen, P., Bao, Y., Jia, W., Hu, C., Zhang, Z.L., Jia, W., 2019a. Discovery of potential biomarkers for osteoporosis using LC-MS/MS metabolomic methods. Osteoporos. Int 30, 1491–1499. https://doi.org/10.1007/s00198-019-04892-0.
Wang, J.M., Yang, J.R., Cheng, X.F., Xiao, R., Zhao, Y.F., Xu, H.M., Zhu, Y.Y., Yan, Z.P., Ommati, M.M., Manthari, R.K., Wang, J.D., 2019b. Calcium alleviates fluoride-induced bone damage by inhibiting endoplasmic reticulum stress and mitochondrial dysfunction. J. Agric. Food Chem. 67, 10832–10843. https://doi.org/10.1021/acs.jafc.9b04295.
Wang, J.M., Xu, H.M., Cheng, X.F., Yang, J.R., Yan, Z.P., Ma, H.L., Zhao, Y.F., Ommati, M.M., Manthari, R.K., Wang, J.D., 2020. Calcium relieves fluoride-induced bone damage through the PI3K/AKT pathway. Food Funct. 11, 1155–1164. https://doi.org/10.1039/c9fo02491c.
World Health Organization, W.H., 2017. Guidelines for drinking-water quality, 4th edition, incorporating the 1st addendum.Available at ⟨https://www.who.int/publications/i/item/9789241549950⟩.
Wu, Z., Hou, Y., Dai, Z., Hu, C.-A.A., Wu, G., 2019. Metabolism, nutrition, and redox signaling of hydroxyproline. Antioxid. Redox Sign 30, 674–682. https://doi.org/10.1089/ars.2017.7338.
Yadav, A., Kumari, N., Kumar, R., Kumar, M., Yadav, S., 2023. Fluoride distribution, contamination, toxicological effects and remedial measures: a review. Sust. Water Resour. Man 9, 150. https://doi.org/10.1007/s40899-023-00926-y.
Yang, F., Wang, L.K., Li, X., Wang, L.W., Han, X.Q., Gong, Z.J., 2014. Sodium butyrate protects against toxin-induced acute liver failure in rats. HEPATOB PANCREAT DIS 13, 309–315. https://doi.org/10.1016/S1499-3872(14)60044-8.
Zhang, A.H., Sun, H., Wang, X.J., 2012. Serum metabolomics as a novel diagnostic approach for disease: a systematic review. Anal. Bioanal. Chem. 404, 1239–1245. https://doi.org/10.1007/s00216-012-6117-1.
Zhang, L., Alfano, J.R., Becker, D.F., 2015. Proline metabolism increases katg expression and oxidative stress resistance in Escherichia coli. J. Bacteriol. 197, 431–440. https://doi.org/10.1128/JB.02282-14.
Zhao, S., Guo, J., Xue, H., Meng, J., Xie, D., Liu, X., Yu, Q., Zhong, H., Jiang, P., 2022. Systematic impacts of fluoride exposure on the metabolomics of rats. Ecotoxicol. Environ. Saf. 242, 113888 https://doi.org/10.1016/j.ecoenv.2022.113888.
Zhong, N., Yao, Y.J., Ma, Y.Z., Meng, X.Y., Sowanou, A., Pei, J.R., 2021. Effects of fluoride on oxidative stress markers of lipid, gene, and protein in rats. Biol. Trace Elem. Res. 199, 2238–2246. https://doi.org/10.1007/s12011-020-02336-z.